Volume 16
Number 48
28 December 2025
Pages 22783–23410

Chemical Science

rsc.li/chemical-science

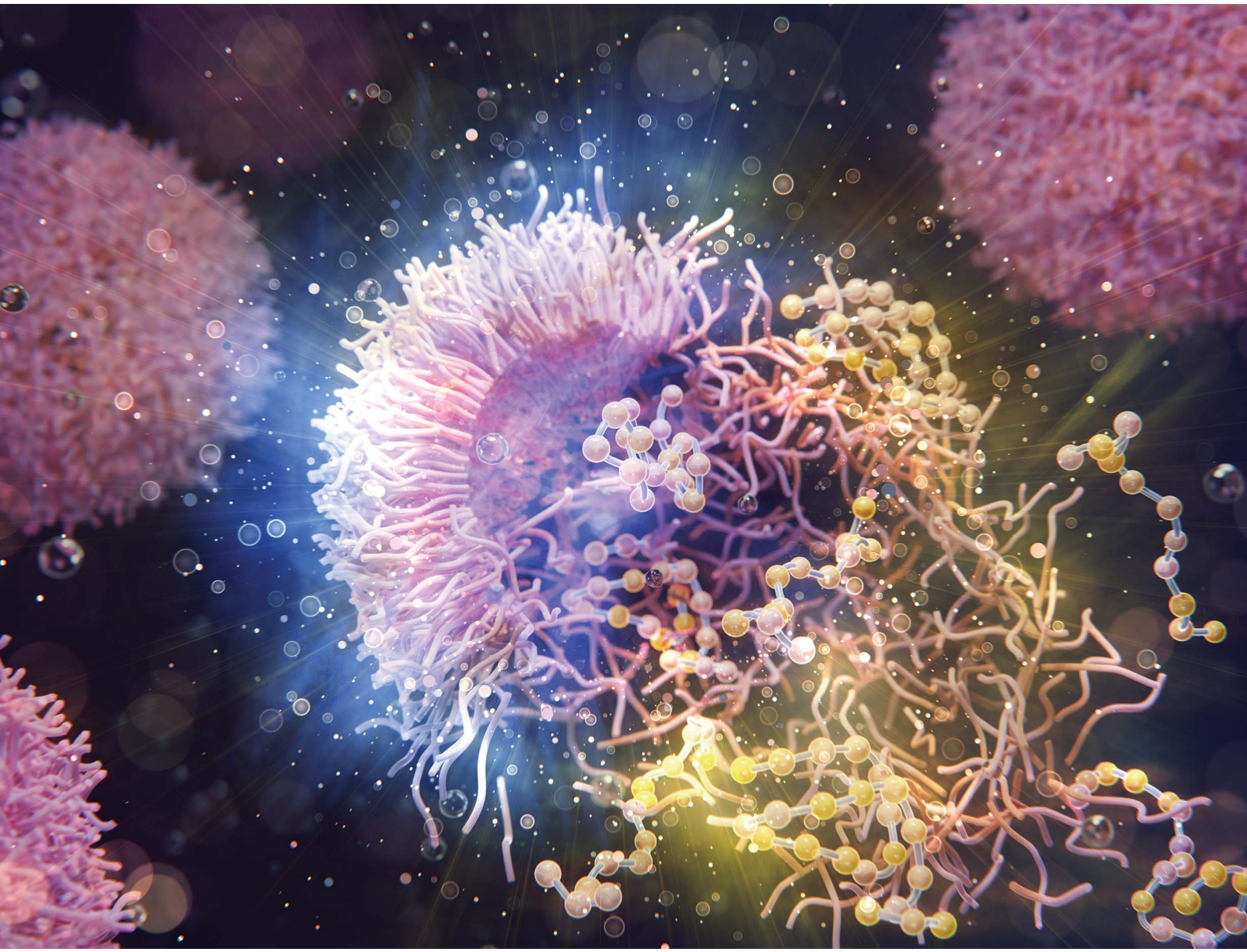

ISSN 2041-6539

ROYAL SOCIETY OF CHEMISTRY

EDGE ARTICLE
Chris Ritchie, Georgina K. Such *et al.*
Monitoring structural change and drug release of responsive nanoparticles using polarity-sensitive fluorophores

15 YEARS ANNIVERSARY

Chemical Science

ROYAL SOCIETY OF CHEMISTRY

EDGE ARTICLE

View Article Online
View Journal | View Issue

Cite this: *Chem. Sci.*, 2025, **16**, 22933

All publication charges for this article have been paid for by the Royal Society of Chemistry

Monitoring structural change and drug release of responsive nanoparticles using polarity-sensitive fluorophores

Yanting Gao,[ab] Peter W. McDonald,[b] Chris Ritchie *[b] and Georgina K. Such *[a]

Received 26th May 2025
Accepted 30th September 2025

DOI: 10.1039/d5sc03803k

rsc.li/chemical-science

Stimuli-responsive polymeric nanoparticles hold significant promise for enhancing the delivery of therapeutic agents, particularly peptides and other small biomolecules. To improve the efficiency of these drug delivery systems, accurate knowledge of their structural dynamics, disassembly process, and loading/release behavior is vital. Amongst a myriad of fluorescent probes utilized for this purpose, environmentally responsive fluorophores demonstrate distinctive advantages due to significant changes in fluorescence intensity, lifetime and/or emission wavelength with variation in their environment. In this work, we designed a series of novel multifunctional probe molecules, isoquinoline betaines (IQBs), with exquisite solvatofluorochromic properties. Through both a steady absorption signal in the visible wavelength range, and an environmentally dependent emission, these IQBs are a powerful tool for simultaneously tracking multiple key processes, including nanoparticle formation and disassembly, the loading and distribution of drug molecules, and the responsive release of drugs. This novel fluorescent probe was covalently conjugated to a pH-responsive nanoparticle and successfully probed the nanoparticle's internal structural rearrangement while also monitoring its drug-release activity of a model peptide in real-time. This IQB fluorescent probe system enhances our understanding of how nanoparticles interact with both their cargo and microenvironment and thus represents an important step forward in the development of more efficient drug delivery systems.

Introduction

Over the past several decades, nanoparticle-based drug delivery systems (DDSs) have emerged as a viable pro-drug technology to overcome the drawbacks of unencapsulated therapeutics, such as poor stability as well as a lack of target specificity.[1,2] The development of efficient DDSs requires several important considerations: (i) they can encapsulate various therapeutics using simple and reproducible techniques and effectively protect them during the delivery process; (ii) they can release cargo under targeted conditions in response to an external or internal trigger; (iii) they allow monitoring of drug release profiles in real time for investigation of drug delivery efficiency. In this regard, polymeric nanoparticles are promising DDSs as they can potentially satisfy all of the above attributes, possess good biocompatibility, and are readily engineered to incorporate stimuli responsiveness.[3,4]

Many stimuli have been investigated to induce specific cargo release for DDSs including endogenous stimuli like redox potential, pH, or enzyme concentration, or external stimuli such as light.[5,6] However, pH variation has sparked particular interest among these variables due to its considerable potential for targeted tumour and intracellular delivery. It is known that pH values vary significantly between physiologically healthy and diseased cells. Tumours exhibit low pH values ranging from 6.4 to 6.8 due to their acidic microenvironment, meanwhile, normal tissue is around 7.4.[7–10] An even greater pH difference is associated with the cellular internalization process. Late endosomes and lysosomes, where nanoparticles are typically trafficked to when internalized, have much lower pH, in the range 4.7–5.5.[11] Thus, pH is a useful trigger to induce site-specific release in these regions.[12,13]

Charge-shifting polymers are commonly used building blocks to design and construct pH-responsive nanoparticles as they can be protonated and consequently display a notable increase in hydrophilicity at pH values below their pK_a, usually leading to nanoparticle disassembly and delivery of their payload.[14–16] Previously, we reported that polymeric core–shell nanoparticles containing two charge-shifting polymers, poly(2-diethylamino ethyl methacrylate) (PDEAEMA) and poly(2-diisopropylamino ethyl methacrylate) (PDPAEMA), can disassemble at low pH (<7.0) and also show ability to traffic into the cytosol from endosomal/lysosomal compartments, a process called endosomal escape.[17–19] Furthermore, the disassembly pH can be modulated by varying the ratio of DEAEMA to DPAEMA

[a]*School of Chemistry, The University of Melbourne, Parkville, 3010, Victoria, Australia. E-mail: gsuch@unimelb.edu.au*

[b]*School of Chemistry, Monash University, Clayton, 3800, Victoria, Australia. E-mail: chris.ritchie@monash.edu*

units in the core polymers, leveraging their respective pK_a values of approximately 7.0 and 6.4.[20] The tunable transition pH and endosomal escape capabilities indicate these constructs have great potential as nanoparticle-based DDSs.

A critical step in the design of delivery systems is understanding the mechanism and efficiency of cargo release. Thus, there is a significant body of research focusing on developing techniques to monitor real-time drug loading and release.[21,22] The most widely used techniques involve fluorescent drugs or fluorophore-labelled drugs.[23] For instance, doxorubicin (DOX) is a widely known anticancer drug that is intrinsically fluorescent, thus it enables the loading and release process to be tracked without chemical modifications.[24] In terms of fluorophore-labelled drugs, a frequently adopted strategy is the attachment of a therapeutic agent to Cy5, a cyanine dye known for its red fluorescence. This conjugation with Cy5 facilitates the non-invasive monitoring of drug release through fluorescence imaging techniques.[25]

Recently, there has been a growing interest in incorporating environmentally sensitive fluorescent molecules into DDSs,[26,27] and designing DDSs with switchable (on/off) fluorescent signals, such as Förster resonance energy transfer (FRET)-based nanocarriers.[28–30] These approaches provide a precise method for monitoring therapeutic agent delivery in real time.[31] Such DDSs are constructed using covalent or non-covalent bonding strategies to integrate organic or inorganic fluorescent materials, enabling controlled fluorescence activation or quenching in response to environmental changes.[32] Although existing methods can elegantly track host–guest interactions, they fall short in monitoring the structural integrity of the host nanoparticle or the subtle changes in the microenvironment that occur prior to disassembly. This is critical for understanding premature drug release or adverse nanoparticle interactions. To address this, we incorporated our recently developed, highly environmentally sensitive IQB fluorophore into our charge-shifting DDS using two complementary strategies: direct incorporation into the particles and guest molecule conjugation. This fluorophore enables effective tracking of nanoparticle behaviour through notable Stokes shift and fluorescence intensity changes within the established pre-disassembly pH

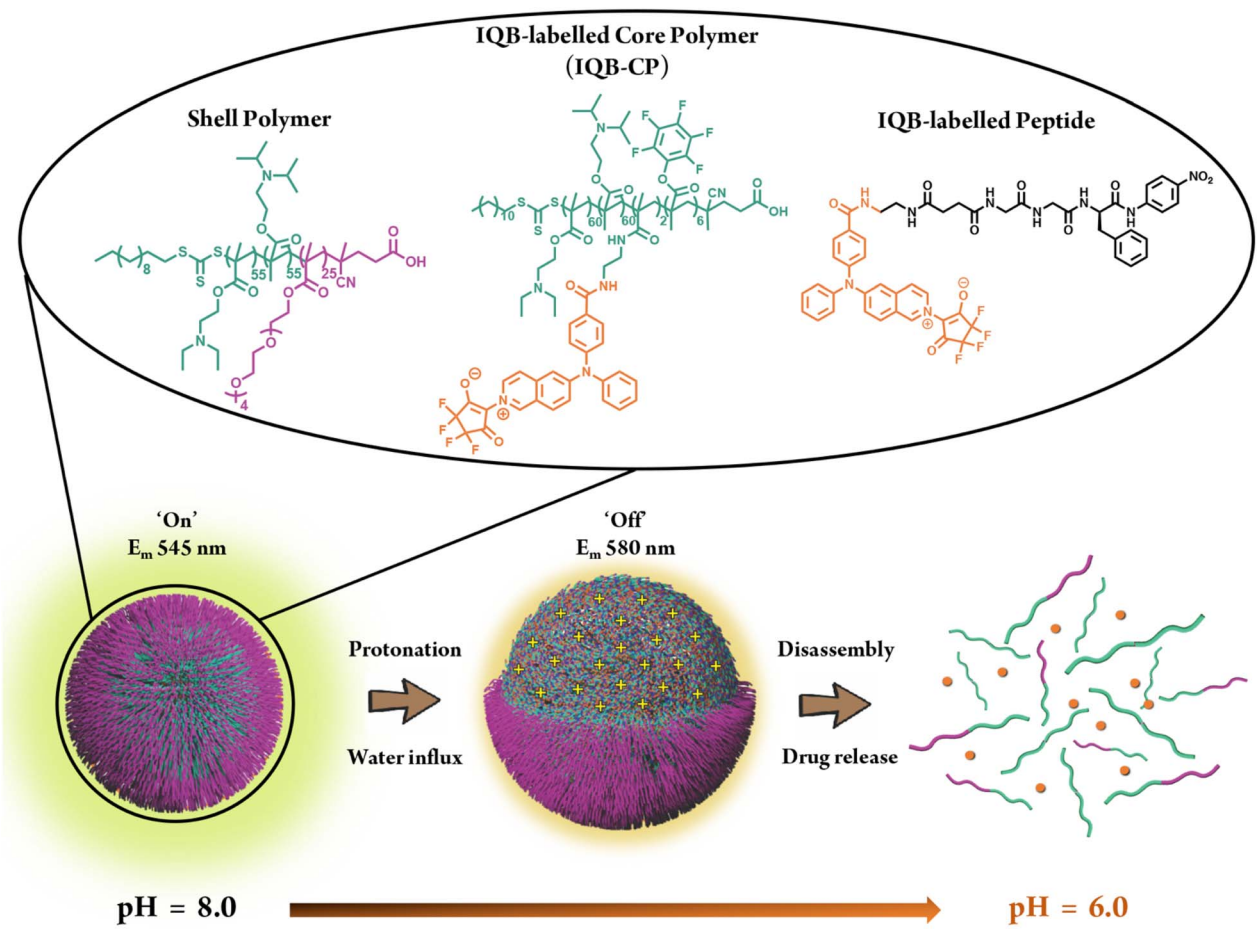

Fig. 1 Schematic illustration of the IQB-labelled pH-responsive nanoparticles comprising the amphiphilic shell polymer, P(PEGMA-*b*-(DEAEMA-*r*-DPAEMA)), charge-shifting core polymer, P(DEAEMA-*r*-DPAEMA-*r*-IQBMA-*r*-PFPMA), and the IQB modified model peptide, IQB-Suc-Gly-Gly-Phe-pNA. These stimuli-responsive nanoparticles exhibit switchable fluorescence, from strong green emission (E_m 545 nm) at pH 8.0 to weak yellow emission (E_m 580 nm) in acidic conditions, indicating the hydrophilic transition within the nanoparticles. Concurrent release of the IQB-labelled model peptide *via* the disassembly of the nanoparticles at endosomal pH, is monitored by UV-vis absorption spectroscopy.

range of our polymeric nanoparticles (Fig. 1). This study complements the limited existing examples that have investigated biomolecular interactions or organizational changes by monitoring fluorescence signal variations in response to shifts in microenvironment polarity or rigidity.[33–37]

Herein, we report an innovative system which combined charge-shifting polymers and environmentally sensitive fluorophores within a single DDS to explore the cascade of events initiated by acidification. We demonstrate the highly versatile nature of this fluorophore by showing it could be used to probe changes of particle hydrophilicity as well as cargo encapsulation and release using a model peptide (betaine modified Suc-Gly-Gly-Phe-pNA). Peptide-based drugs have been identified as a potential new generation of therapeutic molecules as they have many advantages over synthetic drugs, however they are limited by low stability thus making DDSs an attractive delivery method. In this work, it was shown peptide cargo was localized in the hydrophobic core, with efficient release only after particle disassembly.

The IQB fluorophore designed for this study possesses an asymmetric donor–acceptor–donor′ (D–A–D′) architecture (see Scheme 1), with significant intramolecular charge transfer (ICT) following excitation, likely accompanied by significant structural reorganisation giving rise to the desirable photophysical properties required for this investigation. These compounds are related to previously reported pyridinium betaines,[38–41] with the isoquinoline core being incorporated herein to demonstrate the retention of desirable photophysics while achieving red-shifted absorption spectra which is preferred for DDSs. This system provides an integrated approach for directly observing and understanding the structural dynamics of polymer-based DDSs and the interaction of these systems with their cargos, potentially leading to the design of more effective DDSs.

Results and discussion

Synthesis and characterisation of IQBs

The synthesis of IQBs (Scheme 1) involved two Buchwald–Hartwig aminations to construct an asymmetrically functionalized isoquinoline scaffold. Initially, aniline was coupled with 6-bromoisoquinoline to form *N*-phenylisoquinolin-6-amine (**2**), which was subsequently reacted with methyl 4-bromobenzoate (**1**) to yield compound (**3**). Compound (**3**) was then reacted with octafluorocyclopentene in the presence of water to generate **IQB-1**, featuring an ester group. Hydrolysis of the ester produced the corresponding acid (**IQB-2**), which was converted to an amide linkage using mono-BOC-protected ethylenediamine to yield (**IQB-3**). Finally, deprotection afforded the amine-functionalized (**IQB-4**), used in all further reactions. All compounds were characterised by ^{1}H and ^{19}F NMR (Fig. S1–S10).

The normalized UV-vis absorption and fluorescence spectra of (**IQB-1**) in four solvents of varying dielectric constant (toluene – Tol; dichloromethane – DCM; acetonitrile – ACN; and methanol – MeOH; lambda max of the emission – E_m) were recorded and are provided in Fig. 2 (corresponding data for the ester precursor (**3**) are given in Fig. S13 and Table S1). **IQB-1** exhibits a broad absorption band between 380 and 500 nm, showing only slight negative solvatochromism across the four tested solvents. This contrasts sharply with its pronounced positive solvatofluorochromism in the same solvents, as reflected by large Stokes shifts that increase with solvent polarity ($\Delta\lambda_{ST}$;

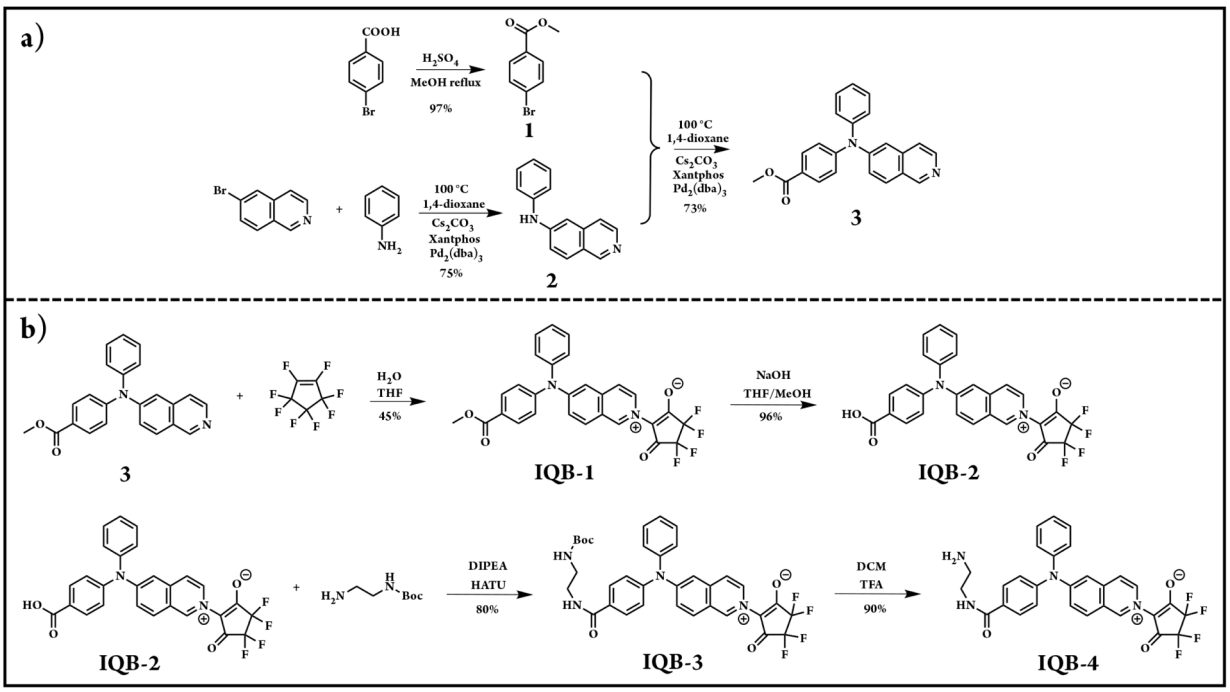

Scheme 1 Synthetic route to (a) an asymmetrically functionalized isoquinoline precursor; and (b) isoquinolinium betaines (IQB 1–4).

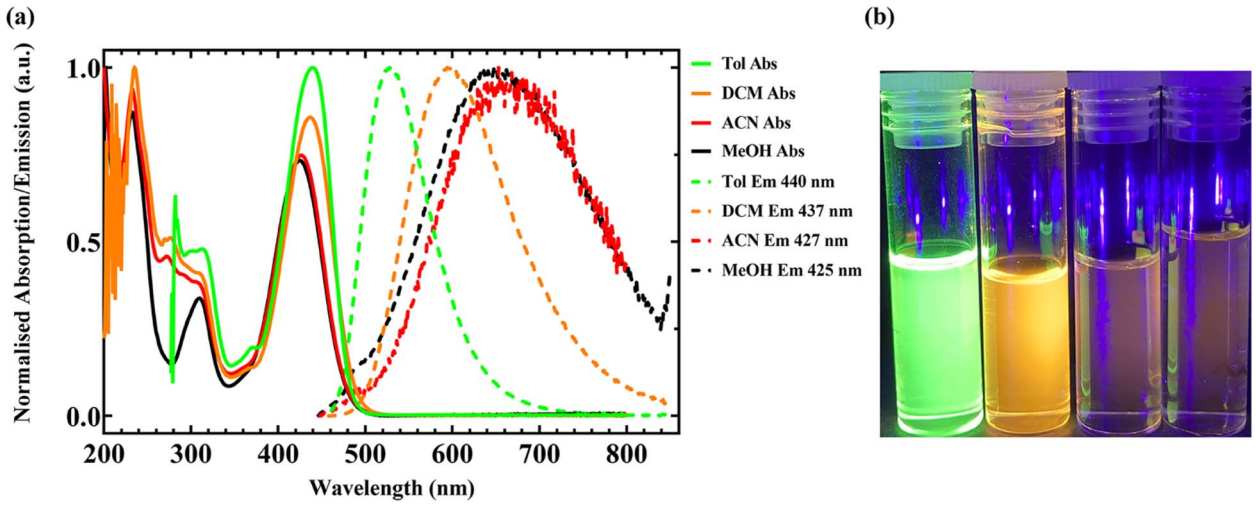

Fig. 2 Solvatofluorochromic properties of **IQB-1** (10 μM). (a) Normalised absorption and emission spectra of **IQB-1** (Green – toluene (Tol); orange – dichloromethane (DCM); red – acetonitrile (ACN); black – methanol (MeOH)). All spectra were normalized to their respective maximum intensities to facilitate comparison of spectral shapes across different solvent conditions. (b) Visual images of **IQB-1** fluorescence under 395 nm excitation (from left to right: Tol, DCM, ACN and MeOH).

Table 1 Photophysical properties for **IQB-1**

Solvent	Tol	DCM	ACN	MeOH
A_m (nm)	439	437	427	425
E_m (nm)	528	594	653	648
$\Delta\lambda_{ST}$ (nm)	89	157	226	223
τ (ns)	5.62	3.69	<0.10	<0.10
PLQY	0.56	0.16	<0.01	<0.01
ε_{max} (M^{-1} cm^{-1})	37 690 (439)	40 680 (437)	38 220 (427)	37 110 (425)

toluene: 89 nm, acetonitrile: 226 nm). Additional photophysical data, including molar absorptivities, quantum yields and fluorescence lifetimes are summarized in Table 1. The radiationless decay/fluorescence quenching observed is also common in such compounds with large geometry changes in the excited state, such as twisted intramolecular charge transfer (TICT) states.[42,43] In this case, twisting of the single C–N bond connecting the intramolecular donor (diphenylamine) and acceptor (isoquinolinium) would generate a relaxed, more twisted conformation and could be responsible for the bathochromic shifts and emission quenching observed.[44] Detailed photophysical interpretation is underway and is out of the scope of this report.

Considering the potential detrimental effects of excitation light with wavelengths below 400 nm (ultraviolet light) on cell viability,[45] the absorption wavelengths of **IQBs 1–4** are more attractive for biological applications. Notably, compared to other commonly used polarity-sensitive fluorescent probes such as Nile Red, these IQB derivatives offer distinct advantages that make them promising candidates for drug delivery applications. First, the ester group at the **IQB-1** position serves as a modifiable site, allowing for convenient conjugation with drug carriers or therapeutic molecules without significantly altering the probe's photophysical properties, thereby enabling versatile functionalization. Second, the absorption wavelengths of **IQBs 1–4** are minimally affected by environmental polarity, facilitating straightforward and reliable monitoring of drug release profiles *ex vivo via* absorption spectroscopy.

Assembly and characterization of IQB attached pH-responsive nanoparticles (IQB@NP)

In this study, the amphiphilic shell polymer (SP), poly(ethylene glycol methacrylate)-*b*-poly(2-(diethylamino)ethyl methacrylate-*r*-2-(diisopropylamino)ethyl methacrylate) P(PEGMA-*b*-(DEAEMA-*r*-DPAEMA)), as well as the charge-shifting core polymer (CP), poly(2-(diethylamino) ethyl methacrylate-*r*-2-(diisopropylamino) ethyl methacrylate-*r*-pentafluorophenyl methacrylate) P(DEAEMA-*r*-DPAEMA-*r*-PFPMA), were synthesized *via* reversible addition–fragmentation chain transfer (RAFT) polymerization (Scheme 2). The charge-shifting monomers, DEAEMA and DPAEMA, are necessary to form pH-responsive nanoparticles, as demonstrated in our previous work.[19] The third component, PFPMA was incorporated into the polymer backbone to enable post-polymerization modification. The molecular weights of SP and CP were determined as approximately 29 kDa and 27 kDa by ^{1}H NMR spectra, and the dispersities ($Đ$) were 1.25 and 1.19 according to Size Exclusion Chromatography (SEC) (Fig. S14–S18 and Table S2).

Post-synthetic modification of the polymers by coupling the charge-shifting CP with **IQB-4** was successful resulting in IQB-CP. Following purification, the conversion ratio of this amide coupling reaction was estimated to be approximately 22%, as determined by the integration ratio between the attached IQB and the residual PFPMA in the ^{19}F NMR spectrum (Fig. S19). The dye-labelled polymer retained the aforementioned responsiveness of IQBs, wherein a marked similarity in absorption and emission spectra was observed ($\Delta\lambda_{ST}$; Tol: 103 nm, ACN: 225 nm) (Fig. S20).

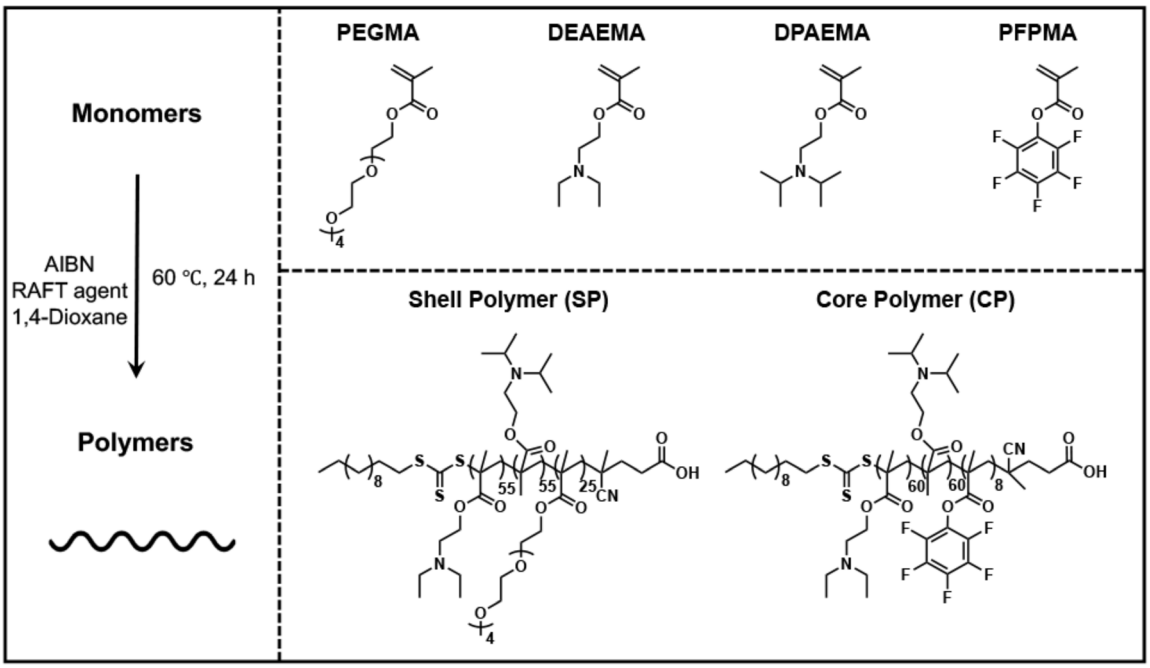

Scheme 2 RAFT polymerization reaction scheme and structures of four different monomers, amphiphilic shell polymer (SP), P(PEGMA$_{25}$-*b*-(DEAEMA$_{55}$-*r*-DPAEMA$_{55}$)), and charge-shifting core polymer (CP), P(DEAEMA$_{60}$-*r*-DPAEMA$_{60}$-*r*-PFPMA$_{8}$).

The covalently incorporated IQB pH-responsive nanoparticles (IQB@NPs) were prepared using a nanoprecipitation method. A 1 : 1 weight ratio of SP and IQB-CP was dissolved in acetone and then precipitated by adding to phosphate-buffered saline (PBS, pH 8.0). Under these conditions, the nanoparticles self-assemble with a core consisting of IQB-CP and the charge-shifting segment of SP, while the PEGMA block of SP remains exposed to the solvent.[46] The resulting particles were purified by dialysis (24 h, MWCO 100 kDa) and filtered through a 0.45 μm polyethersulfone membrane before characterization. The resulting nanoparticles were characterized using dynamic light scattering (DLS), nanoparticle tracking analysis (NTA), and cryogenic transmission electron microscopy (Cryo-EM) to determine their size, distribution, concentration and morphology. While valuable, these techniques require sampling times of multiple minutes and relatively stable dispersions to acquire sufficient data, while being unable to report on small variations within the particle structure. Integration of solvatofluorochromic IQBs into the polymeric matrix presents a complimentary method to monitor the microenvironmental changes within nanoparticles during the pre-disassembly process induced by pH-jump experiments. This approach serves to enhance our understanding of the entire drug release process from initiation to complete disassembly.

The pH-induced disassembly profile of IQB@NPs was analyzed using DLS, where the size and polydispersity of nanoparticles were tracked across a pH range of 8.0 to 5.8 at 37 °C (Fig. 3b) with the disassembly point identified by an abnormal correction function, low particle counts and a high polydispersity index (PDI). Particle destabilization arises from the protonation of the tertiary amines located in the nanoparticle core, leading to increased hydrophilicity, electrostatic repulsion, and ultimately nanoparticle disassembly. The mean size of IQB@NPs increased by 25% from ~160 nm to ~200 nm across the aforementioned pH range, with disassembly complete on reaching pH 6.0 (Fig. 3b). A representative Cryo-EM micrograph showed well-defined spherical nanoparticles with consistent size (~100 nm at pH 8.0), which is slightly smaller than the hydrodynamic diameter indicated by DLS (Fig. 3c). The value of PDI was consistently lower than 0.2, indicating the colloidal stability and monodispersity of the nanoparticles before disassembly.

The nanoparticle analysis suggests subtle nanoparticle swelling before disassembly, indicated by larger particle sizes combined with stable PDI values (<0.2). Therefore, it is reasonable to anticipate perturbation of the local environment within the nanoparticles before disassembly. Understanding this process is critical for designing more stable DDSs, thus we attempted to interrogate this dynamic pre-dissociation process using IQB-labelled CP as a solvatofluorochromic reporter. The emission spectrum of IQB@NPs was determined in the pH range 8.0 to 6.0 using 430 nm as the excitation wavelength and 5 min incubation time (Fig. 3d). A decrease of fluorescence intensity accompanying acidification is observed, along with a red shift of the maximum emission wavelength, from 545 nm at pH 8.0 to 580 nm at pH 6.0. As discussed above, we attribute the intensity changes and distribution shift to the solvatochromic properties, which support a gradual transformation from a hydrophobic to a hydrophilic environment inside the nanoparticles.

Interestingly, the rate of the hydrophobic-to-hydrophilic transition can be correlated with pH and the charge-shifting

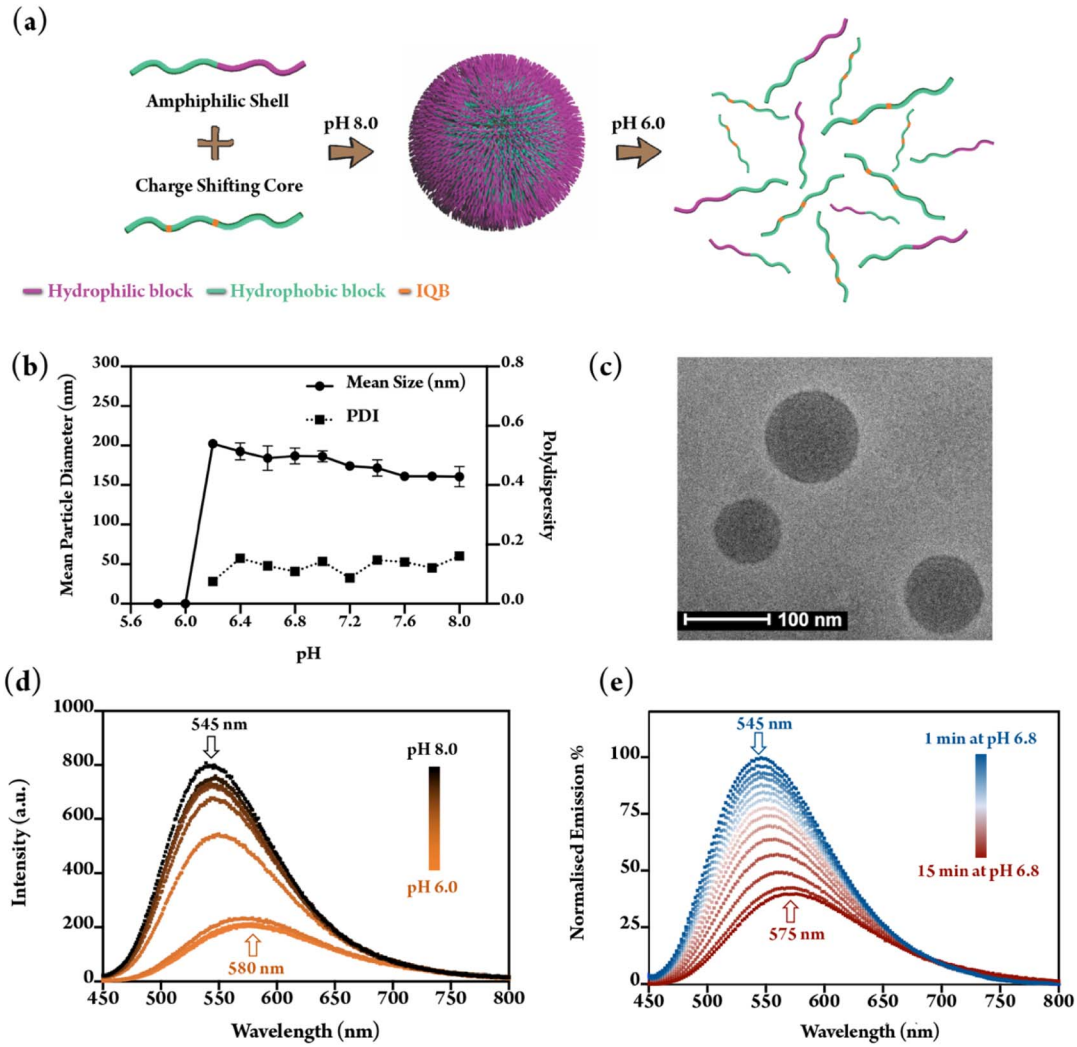

Fig. 3 The formation, dynamic pre-dissociation stage and pH-induced disassembly process of IQB-labelled pH-responsive nanoparticles (IQB@NPs). (a) Graphical representation of the IQB@NPs. (b) Mean diameter (circles) and polydispersity (squares) of IQB@NPs in the pH range 8.0–5.8. (c) Cryo-EM images of IQB@NPs at pH 8.0 (scale bar = 100 nm). Emission spectra of IQB@NPs (d) in the pH range 8.0–6.0; (e) at pH 6.8 within 15 min (E_x = 430 nm).

polymer pK_a. At pH 6.8, the time-dependent emission spectrum demonstrated the transition of IQB@NPs over a 15-minute incubation period (Fig. 3e). Above this pH, the internal environment of the nanoparticles showed only a minor change in polarity within one hour, whereas, below pH 6.8, the particles were observed to transition completely within 1 minute representing greater than an order of magnitude rate enhancement (Fig. S21). The change in kinetics of this hydrophobic-to-hydrophilic transition aligns with the pK_a of the charge-shifting polymers within this system, with intermediate kinetics close to this transition point (pH 6.8). This point can be easily regulated by changing the monomers and their proportions as shown in our previous research.[20] Importantly, this study infers that protonation and therefore changes in the polarity leading to variation in structural and internal particle chemistry occurred well in advance of particle disassembly—an intermediate transition that has not been clearly identified in similar polymeric nanocarriers. Direct tracking of this process by the inclusion of the novel IQB into the core polymer represents the first example of such a study.

Assembly and characterization of pH-responsive nanoparticles loaded with IQB labelled peptides (Pep@NPs)

Peptide-based drugs have been identified as a potential new generation of therapeutic molecules as they have many advantages over synthetic drugs, such as better biocompatibility, lower cytotoxicity and higher selectivity.[47,48] To date, there are more than 50 peptide-based drugs that have reached the market, and hundreds are in active clinical trials and nonclinical studies.[49,50] However, a non-negligible flaw in the application of peptide-based therapeutics is their poor metabolic stability, which is severely limited by the fact that they can be degraded by a myriad of proteases inside the biological environment. Thus, there is considerable interest in the

development of delivery systems that facilitate the encapsulation and protection of peptides before their controlled release at targeted sites.

Currently, most research focuses on the release profile of drug delivery systems, but limited attention is given to the cargo's distribution within the carrier during the encapsulation or understanding the kinetics of drug release. To understand all stages of encapsulation and release of peptide cargo, a betaine peptide was designed and incorporated into the nanoparticle system. The carboxylic acid derivative **IQB-2** was attached to a model peptide (Suc-Gly-Gly-Phe-pNA) through amidation, and the product was confirmed by mass, ^{1}H NMR and ^{19}F NMR spectroscopy (Fig. S11 and S12). Then, IQB-peptide cargos were encapsulated within pH-responsive nanoparticles through nanoprecipitation (Fig. 4a). The purification of obtained Pep@NPs followed the same procedure as described for IQB@NPs above. It is worth noting that, given the model peptide contains only four amino acids and approximately half of the mass of the IQB-peptide conjugate is attributed to the fluorescent dye, the behavior of this IQB-peptide is likely to be strongly influenced by the IQB physical properties. A more systematic study involving different biomacromolecules is currently underway.

Similar to IQB@NPs, Pep@NPs were characterized using DLS, Cryo-EM and fluorescence spectroscopy (Fig. 5). The average size of Pep@NPs slightly increased as the pH decreased according to DLS data (Fig. 5a), ranging from approximately 180 nm at pH 8.0 to around 210 nm at pH 6.2, these values being slightly larger in comparison to IQB@NPs. The particle disassembly point (pH 6.0) and the consistently low values of PDI (below 0.2) suggested no discernible influence attributable to cargo encapsulation. The representative image of Cryo-EM revealed well-defined spherical shapes with an approximate diameter of 110 nm (Fig. 5b). Following dialysis, Pep@NPs showed the characteristic absorption/emission spectra of IQBs (Fig. S22), indicating the encapsulation of these modified biomolecules into the nanoparticles. The emission spectrum was subsequently used to analyze the drug distribution within the nanoparticles before acidification. Pep@NPs displayed the most intense emission signal at pH 8.0, with the peak reaching its maximum around 545 nm (Fig. 5c). This observation aligns with the spectrum obtained from the hydrophobic core of the nanoparticles, as discussed earlier. This result supports the hypothesis that IQB-peptides were located within the hydrophobic pocket, rather than at the interface or attached to shell polymers. The absence of the ^{19}F signal in the NMR spectrum at pH 8.0 which reappears after disassembly at lower pH values

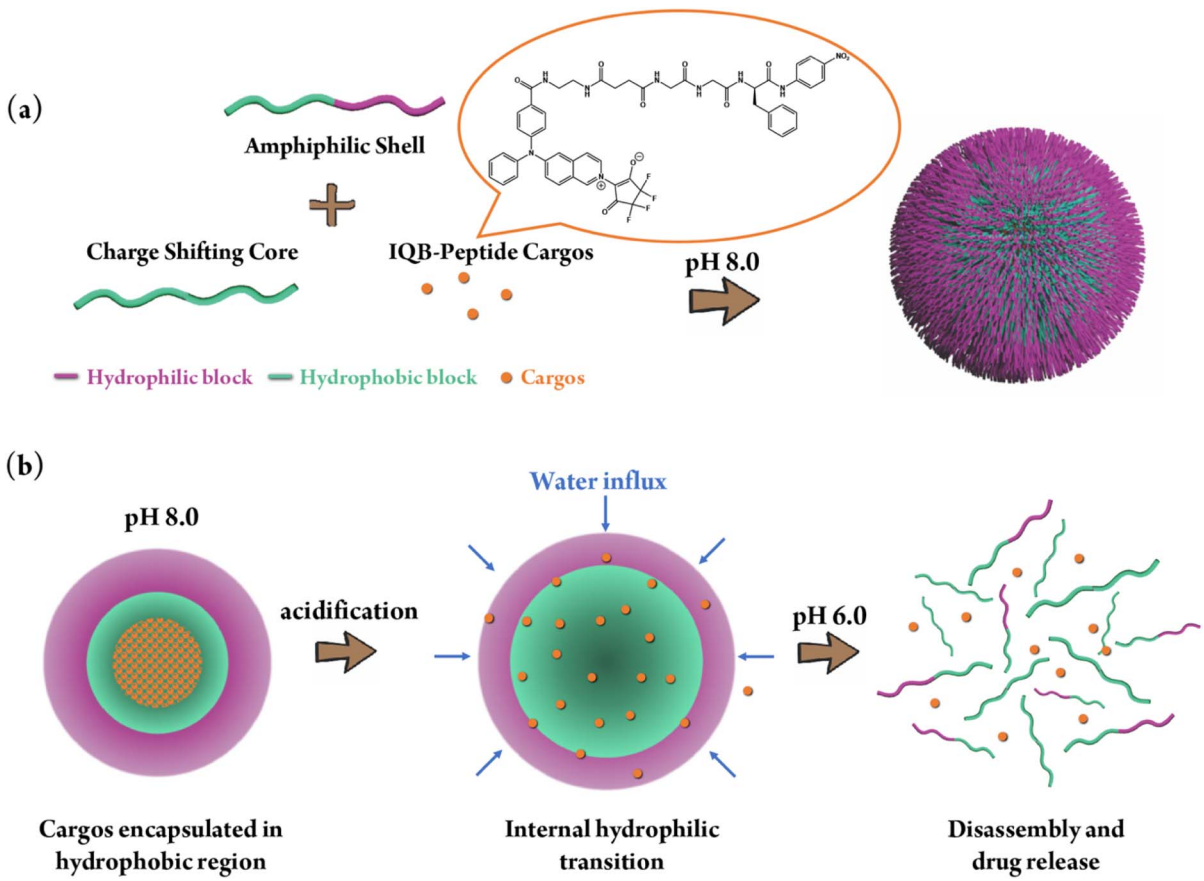

Fig. 4 Graphical representation of the composition of peptide-encapsulated pH-responsive nanoparticles (Pep@NPs) and the proposed mechanism for pH-induced disassembly. Schematic diagram of (a) the formation of Pep@NPs; and (b) three stages of Pep@NPs in response to acidification (cargo-loaded stage, structural rearrangement stage, and drug release stage).

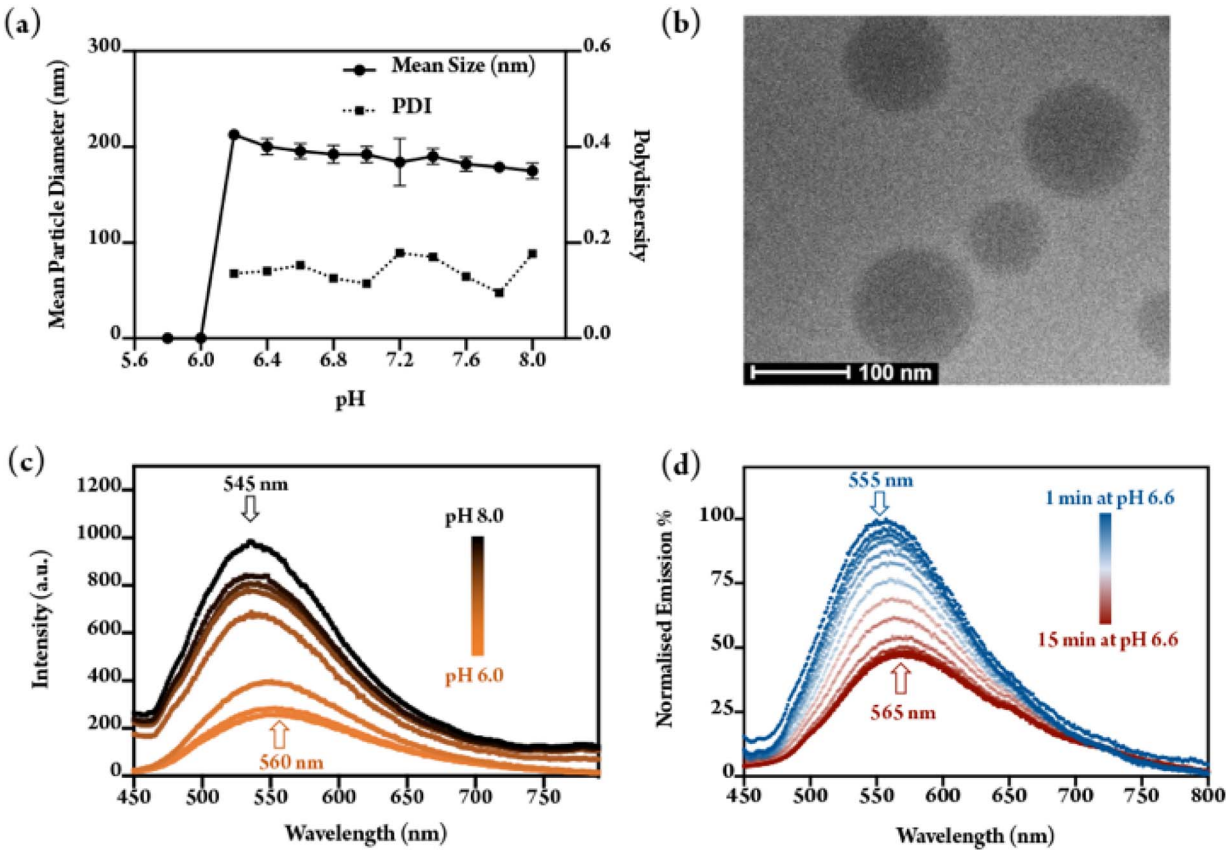

Fig. 5 Properties and morphology of peptide-encapsulated pH-responsive nanoparticles. (a) Mean diameter (circles) and polydispersity (squares) of Pep@NPs in the pH range 8.0–5.8. (b) Cryo-EM images of Pep@NPs at pH 8.0 (scar bar = 100 nm). Emission spectra of IQB@NPs (c) in the pH range 8.0–6.0; and (d) at pH 6.6 within 15 min (E_x = 430 nm).

also supports this conclusion. The inner hydrophobic region of nanoparticles is dense and isolated from the deuterated solvent, leading to significantly shorter spin–spin relaxation times (T2) and the loss of signals in NMR (Fig. S23).[51] Collectively, these results demonstrated that utilizing IQB for cargo labeling provides a straightforward approach to validate successful encapsulation and investigate cargo distribution within the carriers (hydrophobic core or hydrophilic shell) at the initial stage through the corresponding emission spectrum.

As previously explained, the acidification process induced a progressive transformation in the internal environment of these pH-responsive nanoparticles, transitioning from hydrophobic to hydrophilic and ultimately leading to complete disassembly at pH 6.0. The emission spectrum of Pep@NPs demonstrated a similar trend to that observed in IQB@NPs, characterized by a substantial decrease in intensity and a bathochromic shift corresponding to increased polarity (positive solvatofluorochromism) (Fig. 5c). However, despite the identical framework formulations of these two nanoparticles and no variation in the pH of complete disassembly, there was a slight difference in the transition point of the emission spectrum for these two nanoparticles. In contrast to IQB attached to CP through covalent bonds (IQB-CP), the emission spectrum showed that the loaded IQB-peptides were in a polar environment at pH 6.6 instead of pH 6.8. The whole transformation process was completed within 15 minutes, characterized by a 10 nm peak shift (from 555 nm to 565 nm) and approximately a 50% decrease in emission intensity (Fig. 5d). Based on these results, it is suggested that there is a polarity switch within the nanoparticle interior before the carriers disassembled (Fig. 4b). However, no notable emission difference was observed between this intermediate state and complete disassembly, suggesting that peptides were fully exposed to the buffer solution after the transition point. Thus, further investigation into the drug release profile is essential to determine whether peptides were prematurely released from this delivery system at pH values higher than 6.0.

Stability and peptide release tests of Pep@NPs

Prior to conducting the peptide release test, stability assessments of the carriers were undertaken through four hours of DLS measurements. The polydispersity of Pep@NPs at different pH levels remained stable, consistently below 0.2 throughout the duration, indicating there was no evident structural rearrangement (swelling/aggregation) within these carriers (Fig. 6a). In terms of the mean size of the nanoparticles, pH 6.6 exhibited relatively larger sizes compared to pH 7.4 and pH 8.0, aligning with hydrophobic-to-hydrophilic transition discussed earlier.

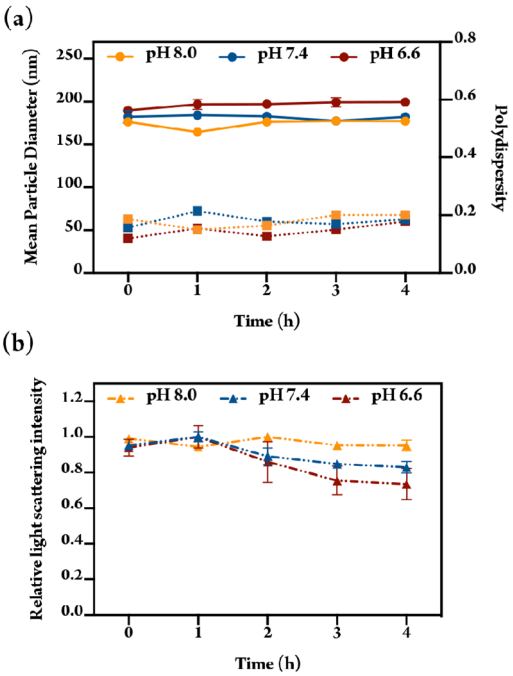

Fig. 6 Stability tests of Pep@NPs at pH 8.0, pH 7.4 and pH 6.6 for 4 h measured by DLS. (a) Mean diameter (circles) and polydispersity (squares); (b) relative light scattering intensity.

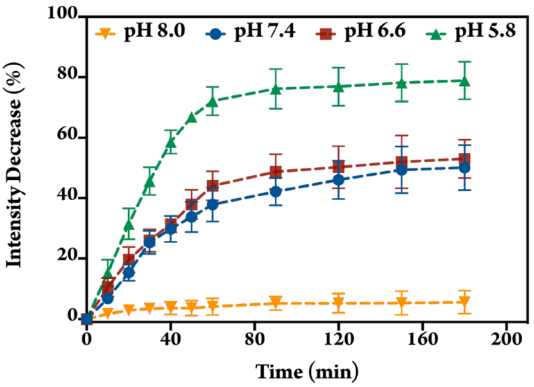

Fig. 7 Model cargo release profile of Pep@NPs at four different pH values (8.0, 7.4, 6.6 and 5.8) measured using UV-vis absorption spectroscopy.

However, no substantial fluctuations were observed for all three samples when maintained at a specific pH, indicative of strong colloidal stability across the pH range from 8.0 to 6.6. Beyond size and polydispersity, the recorded parameter of light scattering intensity was employed to demonstrate changes in nanoparticle concentrations. The intensity of the scattered light is dependent on the size and concentration of analytes.[52] Considering the absence of significant size changes across all samples, the decrease in intensity can be attributed to the loss of nanoparticles in solution. Pep@NPs at pH 8.0 maintained nearly 100% relative intensity after 4 hours of incubation, whereas Pep@NPs at lower pH values exhibited a gradual decline in nanoparticle concentration, approximately 17% for pH 7.4 and 25% for pH 6.6 (Fig. 6b). This decline is attributed to the charge-shifting nature of DPAEMA and DEAEMA monomers, reducing the hydrophobicity of CPs after being partially protonated and thereby compromising the stability of nanoparticles formed through hydrophobic interactions. Based on this data, it is reasonable to assert that Pep@NPs would exhibit sufficient stability in a solution with a pH above 6.6, enabling the investigation of the drug release profile.

Peptide release behavior was examined under simulated biological conditions utilizing the dialysis method.[53] A 5 kDa molecular weight cut-off dialysis tube was employed for a duration of 3 hours, with the buffer being changed every half hour, facilitating the unrestricted diffusion of IQB-peptides (Mw 1 kDa). In contrast to the emission spectrum, which exhibited sensitivity to alterations in surrounding solution polarity, the absorption spectra of IQBs and IQB-modified materials did not show discernible differences in terms of intensity across various solvents (Fig. S24). Hence, the decrease in intensity signified the release of IQB-peptides, transitioning from the nanoparticles to the buffer solution outside the dialysis bag.

As a control, approximately 6% of IQB-peptides were released after 180 minutes at the initial condition (pH 8.0), demonstrating the good stability of Pep@NPs before the protonation of the amine group (Fig. 7). In the corresponding timeframe, approximately 45% of model peptides were lost from nanoparticles at pH 7.4 and pH 6.6, while around 80% of model peptides were released at pH 5.8. It is noteworthy that, despite the pronounced change in the emission spectrum observed at pH 6.6, indicative of buffer influx and hydrophilic transition, this did not lead to a more substantial cargo leakage compared to Pep@NPs at pH 7.4. This suggests that for the size of this cargo the increased hydrophilicity and size of the polymer matrix as a result did not allow for efficient release, this is likely to change with size of cargo or variations in polarity. However, it underscores the challenges with the non-covalent loading of cargo within a polar matrix. Interestingly, the complete release of IQB-peptides was not observed even at pH 5.8. This can be attributed to the partial entrapment of peptides through association with the hydrophobic backbone of polymers, whose molecular weight (~27 kDa) surpasses the cut-off limit of the dialysis bags (5 kDa).

Conclusions

In summary, we have developed pH-responsive IQB-containing nanoparticles, showcasing the capacity for internal structural rearrangement and real-time monitoring of drug release. The newly developed multifunctional fluorophores exhibit environmental sensitivity that allows them to be used to study nanoparticle formation and disassembly, the loading and distribution of drug molecules, and the responsive release of drugs. The pH-responsive nanoparticles in this study were formed by nanoprecipitation, demonstrating pH-induced disassembly observed through DLS. The solvatochromic properties of IQB-labelled CP revealed a gradual hydrophobic to

hydrophilic transformation within the nanoparticles. A transition point at pH 6.8 indicated a rapid transition to a highly polar environment. This is attributed to tertiary amine protonation during charge balancing, causing buffer solution uptake within the nanoparticles. Moreover, a model peptide was modified with **IQB-2** and loaded into pH-responsive nanoparticles (Pep@NPs). The emission spectra demonstrated successful encapsulation and offered insights into cargo distribution and the change of internal environment. The Pep@NPs experienced an internal hydrophilic transition at pH 6.6, prior to their complete disassembly at pH 6.0. In the following drug release assessment, a retention rate exceeding 90% was observed at pH 8.0, while more than 75% of model peptides were released at pH 5.8, indicating promising capability for pH dependent targeted delivery. Notably, despite the notable emission spectrum shift at pH 6.6 indicating hydrophilic transition, it did not result in a considerably greater cargo leakage compared to Pep@NPs at pH 7.4, with approximately 45% of model peptides being released from the nanoparticles at both pH levels. In conclusion, this study presents a versatile fluorescent sensing platform based on polarity-sensitive IQB derivatives for probing nanoparticle structural transitions and *in vitro* drug release behaviours under acidic conditions. While designed as a proof-of-concept, this system lays the groundwork for future optimization toward real-time monitoring and enhanced understanding of environmentally responsive drug delivery systems.

Author contributions

Conceptualisation, Y. G., P. W. M., G. K. S., C. R.; investigation, methodology and data acquisition and curation, Y. G., P. W. M.; writing – original draft preparation, Y. G.; writing – review and editing, all authors; funding acquisition, G. K. S., C. R. All authors have approved the final version of the manuscript and the SI.

Conflicts of interest

There are no conflicts to declare.

Data availability

The data supporting this article have been included as part of the supplementary information (SI). Supplementary information is available. See DOI: **https://doi.org/10.1039/d5sc03803k**.

Acknowledgements

C. R. would like to thank Monash University and the Australian Research Council for funding this research (DP230102664). G. K. S. would like to the thank the Australian Research Council for funding this research (DP240102642). Y. G. would like to acknowledge the support of the University of Melbourne through the Melbourne Research Scholarship and the Dr Albert Shimmins Fund. P. W. M. would like to thank Monash University and the Australian Government for a Research Training Program Scholarship.

References

1 M. J. Mitchell, M. M. Billingsley, R. M. Haley, M. E. Wechsler, N. A. Peppas and R. Langer, *Nat. Rev. Drug Discovery*, 2021, **20**, 101–124.
2 J. K. Patra, G. Das, L. F. Fraceto, E. V. R. Campos, M. D. P. Rodriguez-Torres, L. S. Acosta-Torres, L. A. Diaz-Torres, R. Grillo, M. K. Swamy, S. Sharma, S. Habtemariam and H. S. Shin, *J. Nanobiotechnol.*, 2018, **16**, 71.
3 M. Elsabahy, G. S. Heo, S. M. Lim, G. Sun and K. L. Wooley, *Chem. Rev.*, 2015, **115**, 10967–11011.
4 F. Masood, *Mater. Sci. Eng., C*, 2016, **60**, 569–578.
5 S. Mura, J. Nicolas and P. Couvreur, *Nat. Mater.*, 2013, **12**, 991–1003.
6 G. K. Such, Y. Yan, A. P. Johnston, S. T. Gunawan and F. Caruso, *Adv. Mater.*, 2015, **27**, 2278–2297.
7 B. S. Ashby, *Lancet*, 1966, **2**, 312–315.
8 K. Engin, D. Leeper, J. Cater, A. Thistlethwaite, L. Tupchong and J. McFarlane, *Int. J. Hyperthermia*, 1995, **11**, 211–216.
9 G. Hao, Z. P. Xu and L. Li, *RSC Adv.*, 2018, **8**, 22182–22192.
10 J. Wike-Hooley, J. Haveman and H. Reinhold, *Radiother. Oncol.*, 1984, **2**, 343–366.
11 J. R. Casey, S. Grinstein and J. Orlowski, *Nat. Rev. Mol. Cell Biol.*, 2009, **11**, 50–61.
12 W. Gao, J. M. Chan and O. C. Farokhzad, *Mol. Pharm.*, 2010, **7**, 1913–1920.
13 Z. Ge and S. Liu, *Chem. Soc. Rev.*, 2013, **42**, 7289–7325.
14 N. Deirram, C. Zhang, S. S. Kermaniyan, A. P. R. Johnston and G. K. Such, *Macromol. Rapid Commun.*, 2019, **40**, e1800917.
15 X. Ma, Y. Wang, T. Zhao, Y. Li, L.-C. Su, Z. Wang, G. Huang, B. D. Sumer and J. Gao, *J. Am. Chem. Soc.*, 2014, **136**, 11085–11092.
16 K. Zhou, H. Liu, S. Zhang, X. Huang, Y. Wang, G. Huang, B. D. Sumer and J. Gao, *J. Am. Chem. Soc.*, 2012, **134**, 7803–7811.
17 M. A. Beach, S. L. Y. Teo, M. Z. Chen, S. A. Smith, C. W. Pouton, A. P. R. Johnston and G. K. Such, *ACS Appl. Mater. Interfaces*, 2021, **14**, 3653–3661.
18 U. Nayanathara, B. Rossi Herling, N. Ansari, C. Zhang, S. R. Logan, M. A. Beach, S. A. Smith, N. R. B. Boase, A. P. R. Johnston and G. K. Such, *ACS Appl. Nano Mater.*, 2023, **6**, 10015–10022.
19 A. S. M. Wong, E. Czuba, M. Z. Chen, D. Yuen, K. I. Cupic, S. Yang, R. Y. Hodgetts, L. I. Selby, A. P. R. Johnston and G. K. Such, *ACS Macro Lett.*, 2017, **6**, 315–320.
20 N. Kongkatigumjorn, S. A. Smith, M. Chen, K. Fang, S. Yang, E. R. Gillies, A. P. R. Johnston and G. K. Such, *ACS Appl. Nano Mater.*, 2018, **1**, 3164–3173.
21 Q.-J. Duan, Z.-Y. Zhao, Y.-J. Zhang, L. Fu, Y.-Y. Yuan and J.-Z. Du, *Adv. Drug Delivery Rev.*, 2023, 114793.
22 G. Yang, Y. Liu, J. Teng and C.-X. Zhao, *Biosensors*, 2021, **11**, 505.
23 S. Naghibi, S. Sabouri, Y. Hong, Z. Jia and Y. Tang, *Biosensors*, 2022, **12**, 373.

24 G. Kwon, M. Naito, M. Yokoyama, T. Okano, Y. Sakurai and K. Kataoka, *J. Controlled Release*, 1997, **48**, 195–201.
25 K. Kim, J. H. Kim, H. Park, Y.-S. Kim, K. Park, H. Nam, S. Lee, J. H. Park, R.-W. Park and I.-S. Kim, *J. Controlled Release*, 2010, **146**, 219–227.
26 J. E. Yap, L. Zhang, J. T. Lovegrove, J. E. Beves and M. H. Stenzel, *Macromol. Rapid Commun.*, 2020, **41**, 2000236.
27 S. Chang, X. Wu, Y. Li, D. Niu, Y. Gao, Z. Ma, J. Gu, W. Zhao, W. Zhu and H. Tian, *Biomaterials*, 2013, **34**, 10182–10190.
28 B. Kang, M. M. Afifi, L. A. Austin and M. A. El-Sayed, *ACS Nano*, 2013, **7**, 7420–7427.
29 X. Liang, J. Fan, Y. Zhao and R. Jin, *J. Rare Earths*, 2021, **39**, 579–586.
30 S. Bou, A. S. Klymchenko and M. Collot, *ACS Appl. Nano Mater.*, 2022, **5**, 4241–4251.
31 T. Etrych, O. Janoušková and P. Chytil, *Pharmaceutics*, 2019, **11**, 471.
32 R. T. Kwok, C. W. Leung, J. W. Lam and B. Z. Tang, *Chem. Soc. Rev.*, 2015, **44**, 4228–4238.
33 A. S. Klymchenko, *Acc. Chem. Res.*, 2017, **50**, 366–375.
34 C. Le Droumaguet, O. Mongin, M. H. Werts and M. Blanchard-Desce, *Chem. Commun.*, 2005, 2802–2804.
35 O. A. Kucherak, S. Oncul, Z. Darwich, D. A. Yushchenko, Y. Arntz, P. Didier, Y. Mély and A. S. Klymchenko, *J. Am. Chem. Soc.*, 2010, **132**, 4907–4916.
36 J. Valanciunaite, E. Kempf, H. Seki, D. I. Danylchuk, N. Peyrieras, Y. Niko and A. S. Klymchenko, *Anal. Chem.*, 2020, **92**, 6512–6520.
37 D. I. Danylchuk, S. Moon, K. Xu and A. S. Klymchenko, *Angew. Chem.*, 2019, **131**, 15062–15066.
38 J. Xu, B. Zhang, M. Jansen, L. Goerigk, W. W. H. Wong and C. Ritchie, *Angew. Chem., Int. Ed.*, 2017, **56**, 13882–13886.
39 P. W. McDonald and C. Ritchie, *Chem. Commun.*, 2024, **60**, 3051–3054.
40 P. W. McDonald, J. Xu, D. R. Lonsdale, I. Jones, B. Poggi, R. P. Cox, S. Aloise, A. D. Scully, C. Allain and L. Bodelot, *J. Mater. Chem. C*, 2024, **12**, 19371–19385.
41 P. McDonald, L. Goerigk and C. Ritchie, *Chem. sci.*, 2025, **16**, 15320–15332.
42 W. Rettig, *Angew. Chem., Int. Ed.*, 1986, **25**, 971–988.
43 C. Wang, Q. Qiao, W. Chi, J. Chen, W. Liu, D. Tan, S. McKechnie, D. Lyu, X. F. Jiang and W. Zhou, *Angew. Chem., Int. Ed.*, 2020, **132**, 10246–10258.
44 C. Wang, W. Chi, Q. Qiao, D. Tan, Z. Xu and X. Liu, *Chem. Soc. Rev.*, 2021, **50**, 12656–12678.
45 H. Y. Youn, B. R. Chou, A. P. Cullen and J. G. Sivak, *J. Photochem. Photobiol., B*, 2009, **95**, 64–70.
46 A. S. Wong, S. K. Mann, E. Czuba, A. Sahut, H. Liu, T. C. Suekama, T. Bickerton, A. P. Johnston and G. K. Such, *Soft Matter*, 2015, **11**, 2993–3002.
47 D. J. Craik, D. P. Fairlie, S. Liras and D. Price, *Chem. Biol. Drug Des.*, 2013, **81**, 136–147.
48 A. Varanko, S. Saha and A. Chilkoti, *Adv. Drug Delivery Rev.*, 2020, **156**, 133–187.
49 W. Cabri, P. Cantelmi, D. Corbisiero, T. Fantoni, L. Ferrazzano, G. Martelli, A. Mattellone and A. Tolomelli, *Front. Mol. Biosci.*, 2021, **8**, 697586.
50 A. Henninot, J. C. Collins and J. M. Nuss, *J. Med. Chem.*, 2017, **61**, 1382–1414.
51 C. L. Cooper, T. Cosgrove, J. S. van Duijneveldt, M. Murray and S. W. Prescott, *Soft Matter*, 2013, **9**, 7211–7228.
52 J. Stetefeld, S. A. McKenna and T. R. Patel, *Biophys. Rev.*, 2016, **8**, 409–427.
53 S. S. D'Souza and P. P. DeLuca, *Pharm. Res.*, 2006, **23**, 460–474.